CHEMPHYSCHEM

Supporting Information

Quantitative Resolution of Monomer-Dimer Populations by Inversion Modulated DEER EPR Spectroscopy

Thomas Schmidt, Rodolfo Ghirlando, James Baber, and G. Marius Clore*[a]

cphc_201600726_sm_miscellaneous_information.pdf

EXPERIMENTAL

p66 expression, purification and spin-labeling. The plasmid containing His-tagged HIV-1 reverse transcriptase (p66 subunit) with a HRV 3C protease cleavage site between the tag and the N-terminus of p66 was a gift from Wei Yang.[S1] A cysteine mutation was introduced at either Trp24 or Thr240, and the native cysteine at position 38 was substituted for Ala using the QuickChange Site-Directed Mutagenesis kit (Strategene), resulting in two p66 constructs (W24C/C38A and T240C/C38A), each containing two surface exposed cysteine residues, one at the site of mutation (W24C or T240C) and the other at the native cysteine at position 280.[S2] Expression and purification was carried out as described previously.[S1] Briefly, *E. coli* BL21-DE3 cells bearing the p66 plasmid were grown in minimal medium containing 99% D_2O (Cambridge Isotope Laboratories), 2g/l deuterated (97-98%) d_7-glucose (Cambridge Isotope laboratories), and 1g/l isogro-D powder growth medium (Aldrich) to generate 99% perdeuterated p66. Expression was induced at an A_{600} of 1.0 by addition of 1 mM isopropyl β-D-1-thiogalactopyranoside and grown overnight at 27 ºC. Cells harvested from a 100-mL culture were lysed by sonication in 25 mM Tris-HCl, pH 8, 150 mM NaCl, 20 mM imidazole and 2mM β-mercaptoethanol. The lysate was centrifuged at 20,000 rpm (SS-34 rotor, ThermoFisher Scientific, Asheville, NC) for 30 min at 4 ºC. The supernatant was subjected to affinity chromatography using a Ni-Sepharose High Performance column (GE Healthcare Life Sciences). The column was equilibrated and washed extensively, after passing the lysate, with 50 mM Tris-HCl, pH 8, 800 mM NaCl, 2mM β-mercaptoethanol, and the protein eluted by addition of 300 mM imidazole. Peak fractions were pooled, dialyzed against 25 mM Tris-HCl at pH 8, 150 mM NaCl, 20 mM imidazole, 1mM EDTA, and subjected to HRV 3C protease cleavage overnight at 4 ºC. The cleaved p66 protein was obtained in the flow-through by passing the digest on a Ni-Sepharose High Performance column. The flow-through fraction was incubated with 5 mM dithiothreitol for 1 hr at room temperature, followed by buffer exchange with 50 mM Tris-HCl, pH 8, 400mM NaCl. Spin labeling was accomplished by addition of a 20-fold excess of (1-Oxyl-2,2,5,5-tetramethyl-Δ3-pyrroline-3-methyl) methanethiosulfonate (MTSL, Toronto Research Chemicals) overnight. The reaction mixture was then passed over a Superdex 200 GL (GE Healthcare Life Sciences) column in 50 mM Tris-HCl, pH 8, 800 mM NaCl. Fractions were combined, concentrated and adjusted to give a final protein concentration of 50 μM spin-labeled p66 in 25mM Tris-HCl, pH 8, 400 mM NaCl, 99.9% D_2O and either 30% or 50% deuterated glycerol (99%-deuterated, Cambridge Isotope Laboratories).

Protein A expression, purification and spin-labeling. AviTag-^{C}ProteinA^{C} with cysteine residues introduced closed to the N and C-termini of the native protein A sequence (at positions 39 and 87 of AviTag-Protein A) was expressed purified and labled with MTSL as described previously.[S3]

Extent of spin-labeling and deuteration The level of spin labeling and deuteration was assessed by liquid chromatography (Waters 1500)-positive ion electron spray mass spectrometry (Waters Model LCT). The electrospray data were deconvoluted using the Waters MaxEnt I program from Mass Lynx Version 4.1. In each instance only a single species was observed. For doubly spin-labeled p66(W24C/C280) and p66(T240C/C280) the theoretical molecular weights (100% doubly MTSL spin-labeled and 100% deuterated) are 68,870 and 68,959 Da, respectively, compared to experimental molecular weights of 68,721 and 68,824 Da, respectively. These experimental masses correspond to 100% MTSL-labeling and 97% deuteration.

Pulsed EPR spectroscopy. All pulsed EPR data were collected at Q-band (33.8 GHz) at a temperature of 55 K on a Bruker E-580 spectrometer equipped with a 150W traveling-wave tube amplifier, a model ER5107D2 resonator, and a cryofree cooling unit. Samples were placed in 1 mm internal diameter quartz tubes (Wilmad WG-221T-RB) and flash frozen in liquid nitrogen. Full details of the experimental setups (pulse lengths, pump and observe frequencies, delays, etc…) are provided in the figure legends for the echo-detected spin nutation (Fig. S1) and DEER (Figs. S4 and S7) experiments.

Sedimentation velocity analytical ultracentrifugation. Sedimentation velocity experiments were conducted at 60,000 rpm and 20°C on a Beckman Optima XL-A analytical ultracentrifuge following standard protocols.[S4] Freshly prepared samples of 50 μM p66 in a buffer containing 400 mM NaCl, 25 mM sodium phosphate, pH 6.8, 20 mM $MgCl_2$, 2 mM DTT and 10%, 30% or 50% (v/v) glycerol were loaded in 2-channel, 3 mm path length Epon charcoal filled centerpiece cells. Following temperature equilibration at 0 rpm, the rotor was accelerated to speed and scans were collected using the absorbance detection system at 250 nm over 48 hours. Sedimentation data were time-corrected[S5] and analyzed in SEDFIT 15.01b[S6] in terms of a continuous c(*s*) distribution of Lamm equation solutions with a maximum entropy regularization confidence level of 0.68. To account for the co-sedimentation of glycerol and the accompanying formation of dynamic density and viscosity gradients, an inhomogeneous solvent model was implemented.[S7] The glycerol loading concentration was iteratively refined (manually) during data fitting in the case of samples in 30% (v/v) and 50% (v/v) glycerol. The sedimentation and diffusion coefficients of glycerol at 60,000 rpm and 20°C used in the analysis were determined experimentally by sedimentation velocity of dilute glycerol solutions. These data were collected using the Rayleigh interference optical detection system on a Beckman Coulter ProteomeLab XL-I analytical ultracentrifuge, time-corrected and analyzed in SEDFIT 15.01b[S6] in terms of a single ideal solute. Density and viscosity data files describing these physical properties of aqueous glycerol solutions as a function of concentration were constructed using the coefficients obtained from SEDNTERP (Windows PC version 20111201β),[S8] as described in http://www.analyticalultracentrifugation.com/inhomogenous_solvent.htm. As the coefficients describing the viscosity of glycerol are only valid up to a concentration of 4.252 M (~40% v/v glycerol), viscosity data for aqueous solutions containing 40% (v/v) to 60% (v/v) glycerol were

fitted to an equation for the form $\eta_{glycerol}/\eta_{water} = a + 10^{-3}bC^{0.5} + 10^{-2}cC + 10^{-3}dC^2 + 10^{-3}eC^3$, where C is the molar concentration, to obtain the coefficients *a*, *b*, *c*, *d* and *e*. These were used to construct a viscosity data file used in the analysis of the sample in 50% (v/v) glycerol. The zero order coefficients in the density and viscosity data files correspond to the density and viscosity of 400 mM NaCl, 25 mM sodium phosphate and 20 mM $MgCl_2$, as determined in SEDNTERP (http://sednterp.unh.edu). The protein partial specific volume was determined in SEDNTERP, and excellent data fits were observed with r.m.s.d. values of 0.00424 to 0.00482 A_{250}.

Sedimentation velocity data were also collected for a solution of 50 μM p66 in 400 mM NaCl, 25 mM sodium phosphate (pH 6.8), 20 mM $MgCl_2$ and 2 mM DTT without glycerol. These data were collected on a Beckman Coulter ProteomeLab XL-I analytical ultracentrifuge in 3 mm pathlength cells at 50,000 rpm and 20°C using the using the Rayleigh interference optical detection system. Data were analyzed in terms of a continuous c(*s*) distribution, following time-correction, with excellent fits (0.00501 fringes r.m.s.d.).

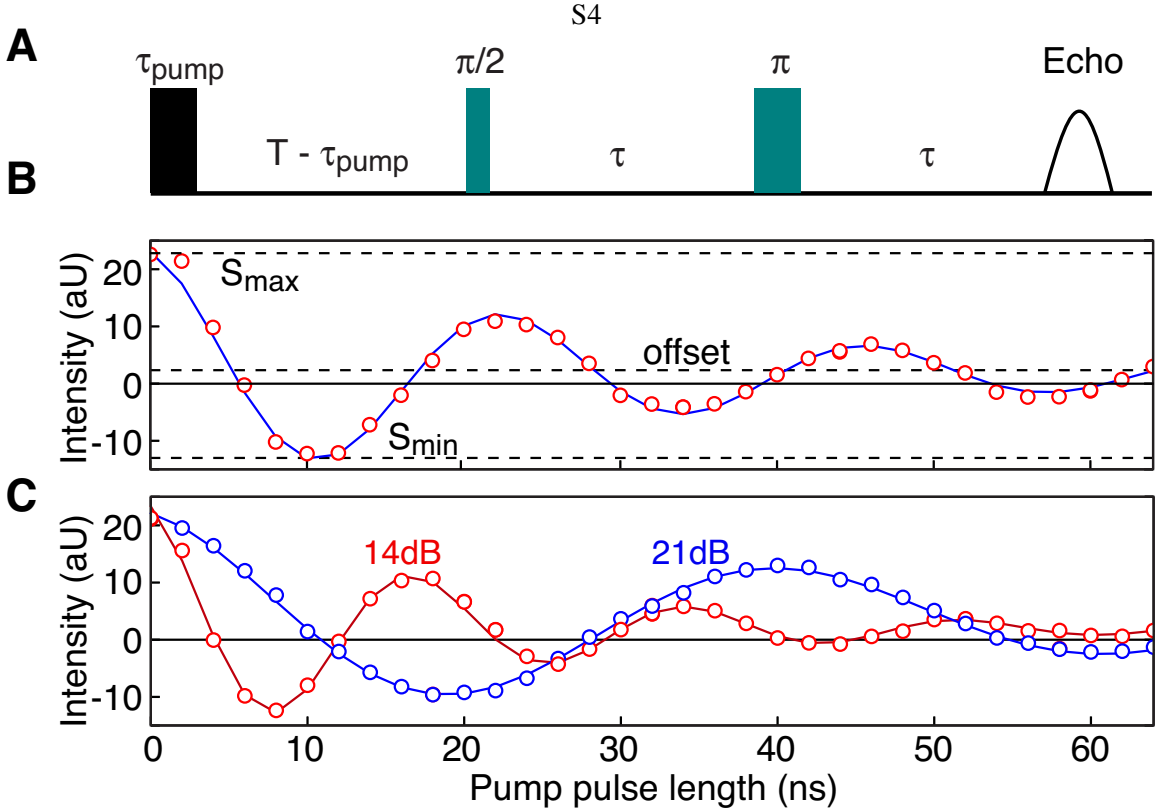

Figure S1. Calibration of 180° ELDOR pulse length and determination of inversion efficiency. (**A**) Echo-detected spin nutation pulse sequence[S9] (T = 350 ns, τ = 400 ns, π/2 and π pulses = 12 and 24 ns, respectively). The length of the pump pulse (τ_{pump}) at any given power was incremented from 0 to 120 ns in 2 ns increments. Each point is a result of 128 repetition shots. The frequency of the pulses was centered at the maximum of the Q-band nitroxide spectrum located at +30 MHz from the center of the resonator frequency. (**B**) Echo amplitude (S) as a function of the length (τ_{pump}) of the pump pulse (attenuation 16 dB) for U-[^{2}H]-p66(T240C/C280) in 30% (v/v) d_8-glycerol 70%(v/v) D_2O. The echo amplitude is given by an empirical exponential damped cosine, $S(\tau_{pump}) = a_0 \cdot \exp(-a_1\tau_{pump}) \cdot \cos(a_3\tau_{pump}) + a_4$, where the parameters a_1 through a_4 are determined by non-linear least-squares fitting. (Note that the offset can be eliminated by phase cycling the π/2 pulse along ±x; ref. S9). The maximum echo amplitude S_{max} is given by $a_0 + a_4$ and is obtained at $\tau_{pump} = 0$; the minimum echo amplitude S_{min} is obtained when τ_{pump} corresponds to a 180° inversion pulse; and a_4 is the offset. The inversion efficiency (λ_{180}) of the 180° pump pulse is calculated from $\lambda_{180} = (S_{max} - S_{min})/2(S_{max} - a_4)$. In the case where the spectrum is broader than the excitation bandwidth, the functional form for the echo amplitude $S(\tau_{pump})$ depends on the lineshape and excitation bandwidth, and for infinite bandwidth is described by a Bessel function. (C) The inversion efficiency is affected by the length of the 180° pump pulse (i.e. the attenuation used for the pump pulse: red, 14 dB, blue 21 dB).

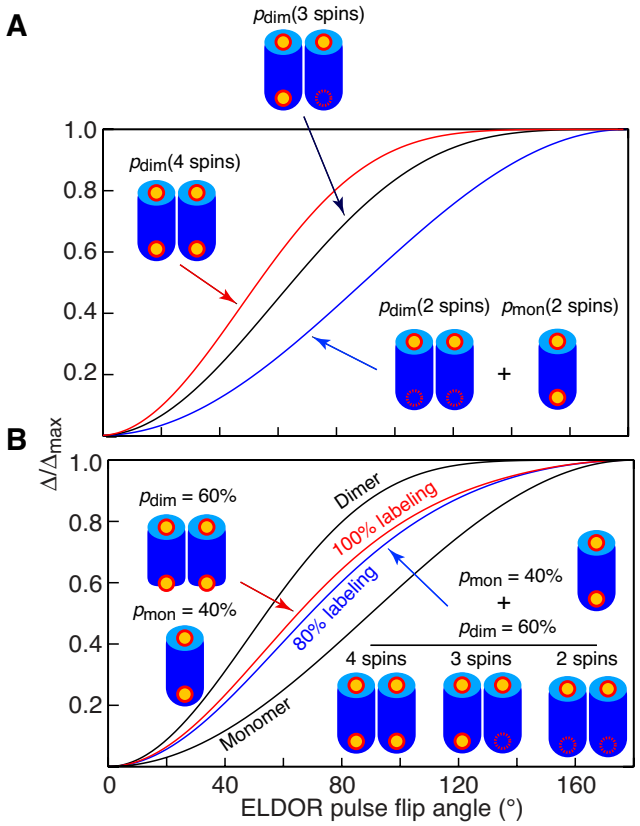

Figure S2. Impact of incomplete spin-labeling the dependence of normalized modulation depth (Δ/Δ_{max}) on ELDOR pulse flip angle. (A) When spin-labeling efficiency is less than 100%, 3 spin dimeric species will also contribute to the normalized modulation depth. (B) Comparison of normalized modulation depth versus ELDOR pulse flip angle for a monomer/dimer equilibrium comprising a population of 60% monomer (p_{mon}) and 40% dimer (p_{dim}) with 100% (red) and 80% (blue) spin-labeling efficiency. The curves for 100% dimer and 100% monomer are shown in black. When spin-labeling is incomplete with fractional labeling f (assumed to be equal for all sites) the populations of one- ($p_{(1)}$), two- ($p_{(2)}$), three- ($p_{(3)}$) and four-spin ($p_{(4)}$) species in a system comprising four labeling sites (e.g. a dimer with doubly-labeled subunits) are given by $p_{(1)} = (1-f)^3$, $p_{(2)} = 3f(1-f)^2$, $p_{(3)} = 3f^2(1-f)$ and $p_{(4)} = f^3$, respectively; for a system with two labeling sites, the populations of one and two-spin species are $p_{(1)} = 1-f$ and $p_{(2)} = f$, respectively.[S9] Thus, with incomplete labeling Eq. (2) in the main text for $(\Delta/\Delta_{max})_{obs}$ has to be modified as follows to include the effect of two- and three-spin dimeric species:

$$(\Delta/\Delta_{max})_{obs} = \frac{[fp_{mon} + 3f(1-f)^2 p_{dim}](\Delta/\Delta_{max})_{N=2} + 3f^2(1-f)p_{dim}(\Delta/\Delta_{max})_{N=3} + f^3 p_{dim}(\Delta/\Delta_{max})_{N=4}}{fp_{mon} + 3f(1-f)^2 p_{dim} + 3f^2(1-f)p_{dim} + f^3 p_{dim}} \quad \text{(S1)}$$

where p_{mon} and p_{dim} are the populations of monomer and dimer, and $p_{dim} = 1 - p_{mon}$. (Note that zero and one-spin species are not included in eq. S1 since they do not contribute to Δ/Δ_{max}.) The labeling efficiency can either be determined independently by liquid chromatography-mass spectrometry, or can be treated as an additional unknown parameter in the fitting procedure. The latter will necessarily reduce the accuracy with which the populations of monomer and dimer can be determined, so it is best to determine f independently.

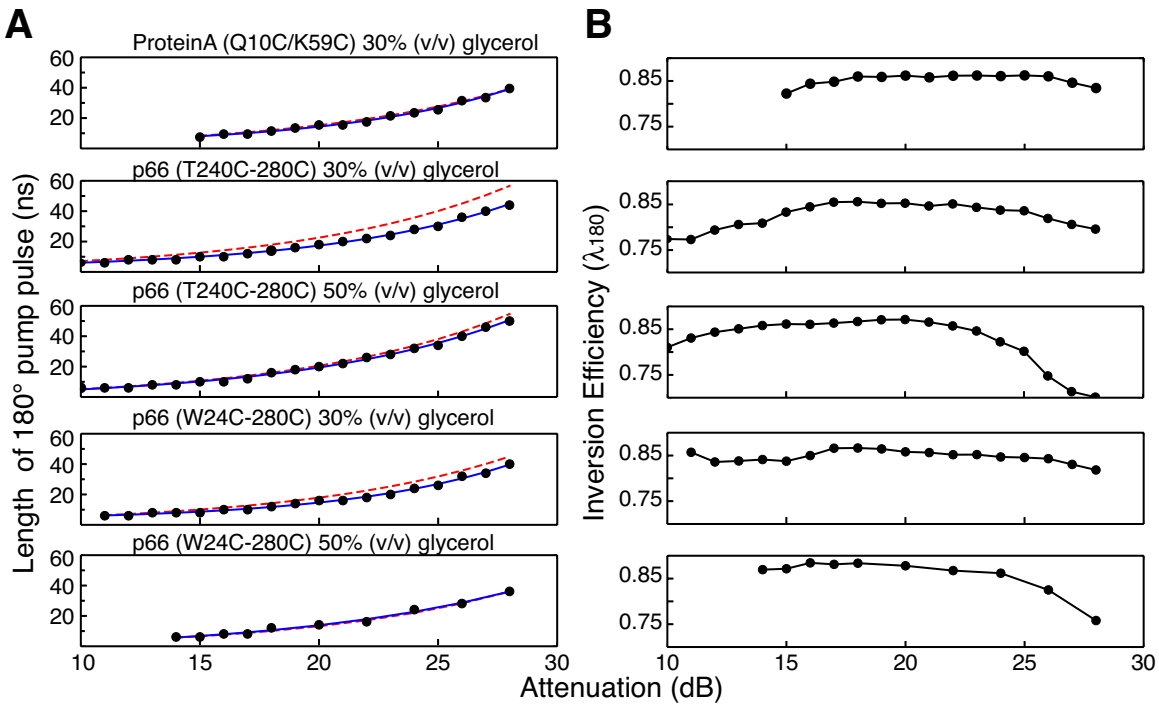

Figure S3. Dependence of (A) the length of the 180° pump pulse and (B) the maximum inversion efficiency (λ_{max}) on the attenuation used for the pump pulse as determined from the spin-echo nutation experiment (cf. Fig. S1). Experimental points are shown as black circles. The red dashed lines in (A) are the theoretical curves of 180° pulse length versus attenuation calculated using the equation $\tau_{pump}(dB_{pump}) = \tau_{pump}(dB_{ref})10^{\Delta dB/20}$, where $\tau_{pump}(dB_{ref})$ is the 180° pump pulse length at the reference attenuation (lowest dB setting), and $\tau_{pump}(dB_{pump})$ is the 180° pulse at a given attenuation (dB_{pump}) setting, and $\Delta dB = (dB_{pump} - dB_{ref})$. Note that deviations between the theoretical (red lines) experimental curves (black circles) are due to non-linearity of the amplifier at the highest power (lowest attenuation) settings. Thus, it is essential to experimentally determine the length of the 180° pump pulse as a function of attenuation. In the DEER experiments attenuation settings for the ELDOR pulse were restricted to experimental λ_{max} values ≥ 0.8.

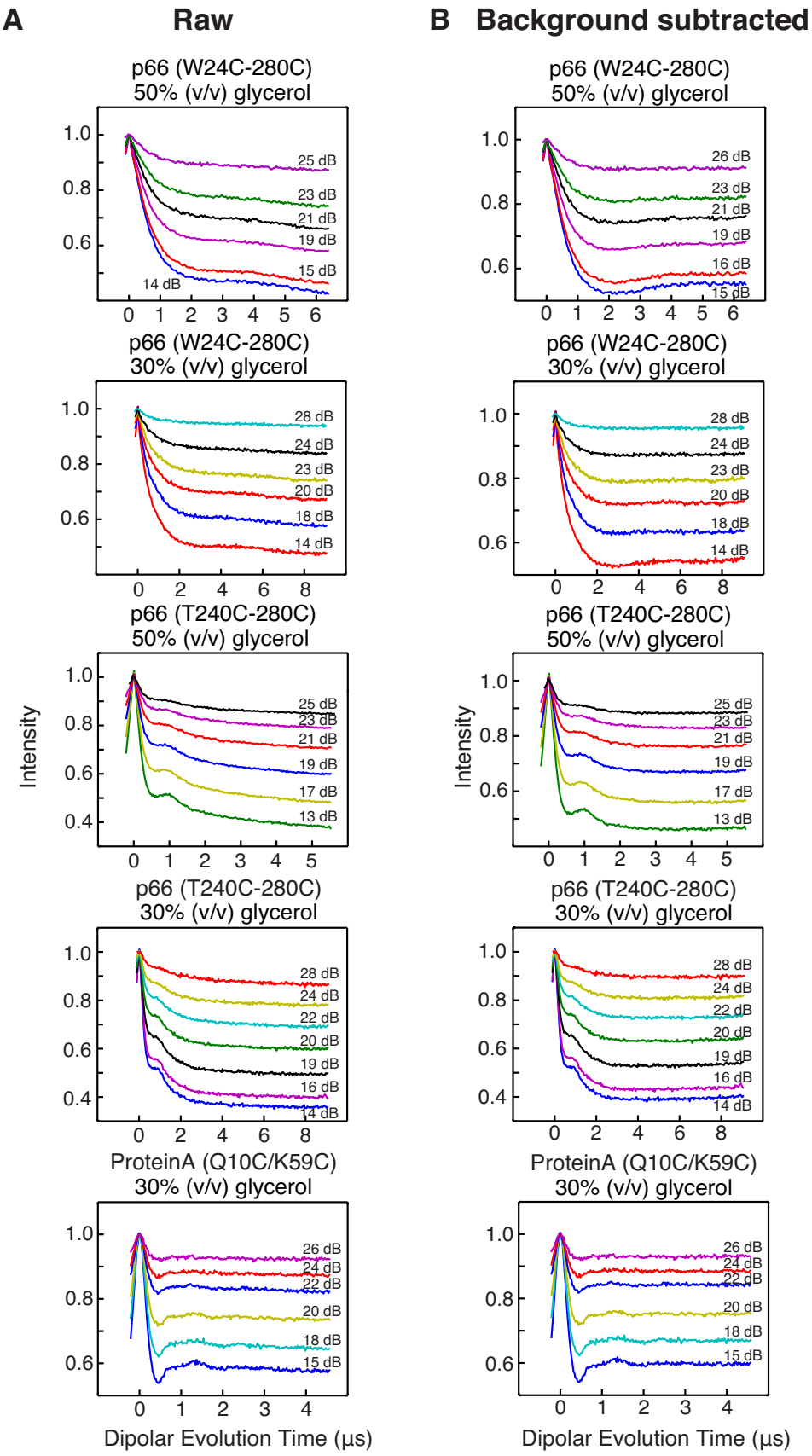
A
Raw
B
Background subtracted
p66 (W24C-280C)
50% (v/v) glycerol
25 dB
23 dB
21 dB
19 dB
15 dB
14 dB
26 dB
23 dB
21 dB
19 dB
16 dB
15 dB
p66 (W24C-280C)
30% (v/v) glycerol
28 dB
24 dB
23 dB
20 dB
18 dB
14 dB
28 dB
24 dB
23 dB
20 dB
18 dB
14 dB
p66 (T240C-280C)
50% (v/v) glycerol
25 dB
23 dB
21 dB
19 dB
17 dB
13 dB
25 dB
23 dB
21 dB
19 dB
17 dB
13 dB
p66 (T240C-280C)
30% (v/v) glycerol
28 dB
24 dB
22 dB
20 dB
19 dB
16 dB
14 dB
28 dB
24 dB
22 dB
20 dB
19 dB
16 dB
14 dB
ProteinA (Q10C/K59C)
30% (v/v) glycerol
26 dB
24 dB
22 dB
20 dB
18 dB
15 dB
26 dB
24 dB
22 dB
20 dB
18 dB
15 dB
Intensity
Dipolar Evolution Time (µs)

Figure S4

Figure S4. Representative (**A**) raw and (**B**) background-subtracted DEER echo curves as a function of ELDOR pulse angle. In the traces shown the ELDOR pulse length is 8 ns and the lowest indicated attenuation setting (i.e. bottom trace) corresponds to the 180° pulse length. To obtain the full range of ELDOR pulse flip angles from 30-40° to 180° shown in the main paper, it was necessary to use three different ELDOR pulse lengths (6, 8 and 10 ns) and attenuation settings as the pulse length and attenuation on our Q-band EPR spectrometer could only be altered in increments of 2 ns and 1dB, respectively. The ELDOR pulse attenuation was incremented from its initial value (13 to 16 dB) for the 180° pulse up to 28 dB with $\lambda_{max} \geq 0.8$. The observe pulse and pump pulses were separated by 90 MHz with observe π and $\pi/2$ pulses of 24 and 12 ns, respectively. The pump frequency was centered at the maximum of the Q-band nitroxide spectrum located at +30 MHz from the center of the resonator frequency. The τ_1 value for the first echo-period time (see Fig. 1a of main text) of 400 ns was incremented eight times in 16 ns increments to average ^{2}H modulation; the position of the pump pulse was incremented in steps (Δt) of 36 ns. The sample temperature was 55 K. The bandwidth of the overcoupled resonator was approximately 120 MHz. DEER curves were sampled up to t_{max} values of 7 or 9 μs for the various ELDOR pump pulse lengths with τ_2 set to t_{max} + 700 ns. Data collection was not carried out over the full τ_2 range because of a persistent "2+1" echo pertubation of the DEER curve at a time of about τ_1 from the final observe π pulse. Data acquisition time for a single trace was ~ 1 h, leading to a total data acquisition time for the complete ELDOR flip angle series of ~30 h. The pulse gate time used for echo integration was 32–38 ns. The DD (a GUI of GLADD; Global Analysis of DEER Data[S10]) homogeneous model with a dimension of 3 (i.e. exponential background) was used to fit and subtract the background. Cutoffs of 6.3 and 6 μs were used to process the p66 (W24C/C280) and p66(T240C/C280) data, respectively, in 50% d_8-glycerol, while cutoffs of 8.5 and 5 μs were used to process the p66 data and the protein A(Q10C/K59C) data, respectively, in 30% d_8-glycerol. It is worth noting that the normalized modulation depth does *not* depend on the spin-label phase relaxation time T_m for the different spins: i.e. changes in T_m due to localized relaxation effects such as protonation do not affect modulation depth.[S3] One can think of the final echo as a convolution of echoes from all spin pairs involved. If one echo of the ensemble becomes smaller because of a shorter T_m, it will still have the same modulation depth but its contribution to the final signal will just effectively be of lower signal-to-noise. In this regard the bimodal distribution of protonated protein A[S3] is relevant: the short distance peak of the $P(r)$ distribution (cf. Fig. 2B) in protonated protein A rapidly disappears as the second echo period of the DEER experiment (cf. Fig. 1A) is increased because of a differential T_m effect, but the modulation depth remains unchanged (cf. panels *g* and *h* of Fig. 2 in ref. S3). Thus, if one spin of say a trimer has a shorter T_m, then its contribution as an observer spin to the signal intensity would be attenuated relative to that of the other two spins although its modulation depth contribution would be the same.

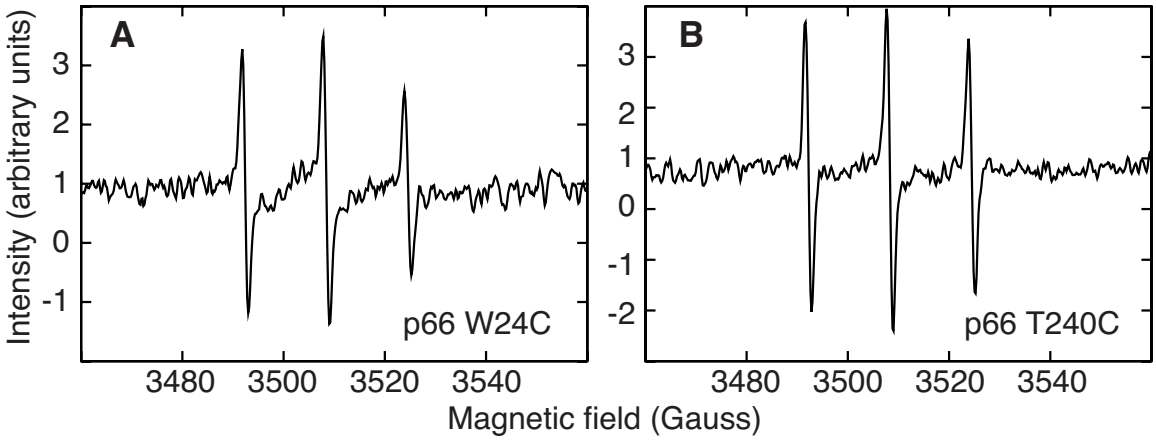

Figure S5. Continuous-wave EPR spectra of MTSL-labeled p66 indicative of mobile MTSL spin-labels. (**A**) p66 W24C/C280 and (**B**) p66 T240C/C280. Spectra were obtained at X-Band with an incident microwave power of 1.5 mW using a Bruker E-580 spectrometer equipped with a traveling-wave tube amplifier and a model ER4118XMD5 probe at room temperature. The two protein samples (50 μM) were in 25mM Tris-HCl, pH 8, 400 mM NaCl, 20 mM MgCl. No glycerol is present.

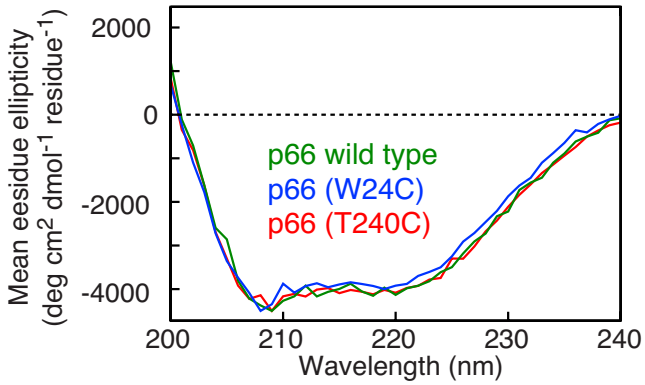

Figure S6. Comparison of circular dichroism spectra of wild type p66 (green) with those of the MTSL-labeled W24C/C38A (blue) and T240C/C38A (red) mutants. No difference in secondary structure is apparent. The CD spectra were recorded at room temperature on 4 μM protein samples in 10 mM potassium phosphate, pH 8 and 100 mM KCl using a Jasco J-810 spectropolarimeter with a 0.01cm path length cell.

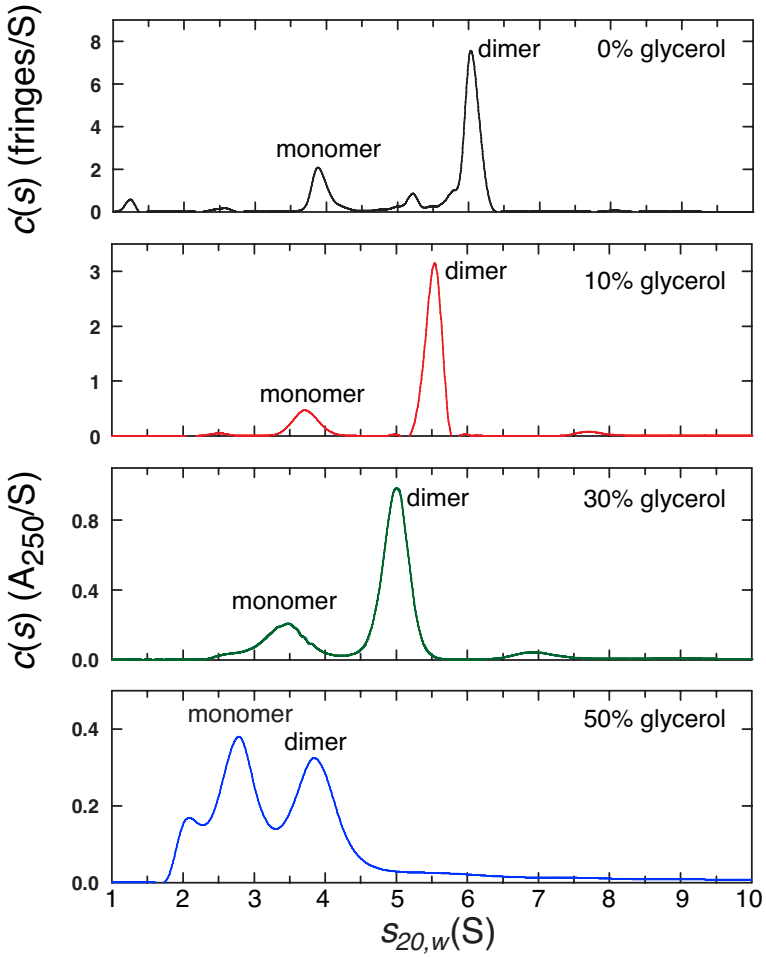

Figure S7. Absorbance c(*s*) profiles for 50 μM p66 in 0%, 10%, 30% and 50% (v/v) gycerol based on sedimentation velocity data. (A) Interference data collected in the absence of glycerol result in a c(*s*) profile showing the presence of two species corresponding to a p66 monomer and dimer (top panel, black curve). Based on the integrated contributions of the signal, monomer and dimer concentrations of 10 μM and 38 μM (in monomer units), respectively, are determined. These correspond to populations of 34% monomer and 66% dimer. (B) Absorbance data collected at 250 nm in the presence of 10% glycerol were first analyzed in terms of a c(*s*) distribution of sedimenting species, without accounting for the dynamic glycerol gradient. Excellent fits were obtained (0.00444 A_{250} r.m.s.d.) resulting in a profile showing the presence of p66 monomer and dimer (second panel, red curve). Based on the integrated signals, approximately 20% of monomer and 80% of dimer are observed, in terms of signal units (Table S1). Accounting for a dynamic gradient with 10% (v/v) glycerol leads to just as good a fit (0.00449 A_{250} r.m.s.d.) with essentially identical proportions of monomer and dimer. Identical populations of monomer and dimer are observed when data are modeled in terms of a dynamic gradient with glycerol concentrations ranging from 8% to 12% (v/v). (C) Data collected in the presence of 30% (v/v) glycerol were modeled in terms of a c(*s*) distribution that accounts for the dynamic glycerol gradient with excellent fits (0.00437 A_{250} r.m.s.d.). The analysis was repeated using a series of glycerol concentrations ranging from 24 - 30% (v/v), and best-fits were observed at 26% (v/v) glycerol (third panel, green curve) with an r.m.s.d. of 0.00420 A_{250}. A larger proportion of monomer was

observed, when compared to data collected at 10% (v/v) glycerol, with approximately 27% of monomer and 73% of dimer, in terms of signal units (Table S1). (D) In a similar manner data collected in 50% (v/v) glycerol were modeled using a range of glycerol concentrations from 46 - 54% (v/v) glycerol. The c(*s*) profiles, now significantly shifted to smaller *s*-values, showed similar proportions of monomer and dimer. Best-fits were obtained at 48% (v/v) glycerol with an r.m.s.d. of 0.00482 A_{250} (bottom panel, blue curve). The proportion of monomer is significantly increased with approximately 55% monomer and 45% dimer, in terms of signal units (Table S1).

Overall, the sedimentation velocity data show that the proportion of p66 monomer increases with increasing glycerol concentration, consistent with observations made by Inversion Modulated DEER EPR. Even though sedimentation data modeling is complicated by the dynamic gradient setup by the co-sedimentation of glycerol, this does not account for all of the phenomena that complicate the physical process of sedimentation. Specifically we have not considered the non-ideal sedimentation and diffusion of glycerol at the high concentrations used, and assumed ideal, low concentration values for the glycerol sedimentation and diffusion coefficients. Furthermore, based on studies carried out on aldolase,[S12] proteins are not necessarily invariant particles in terms of their partial specific volume[S13] and hydration in the presence of different concentrations of glycerol. We have not even attempted to account for these phenomena, which may explain the shift of the c(*s*) profile to smaller *s*-values in the presence of increasing glycerol concentrations, and that becomes quite pronounced at 50% (v/v) glycerol.

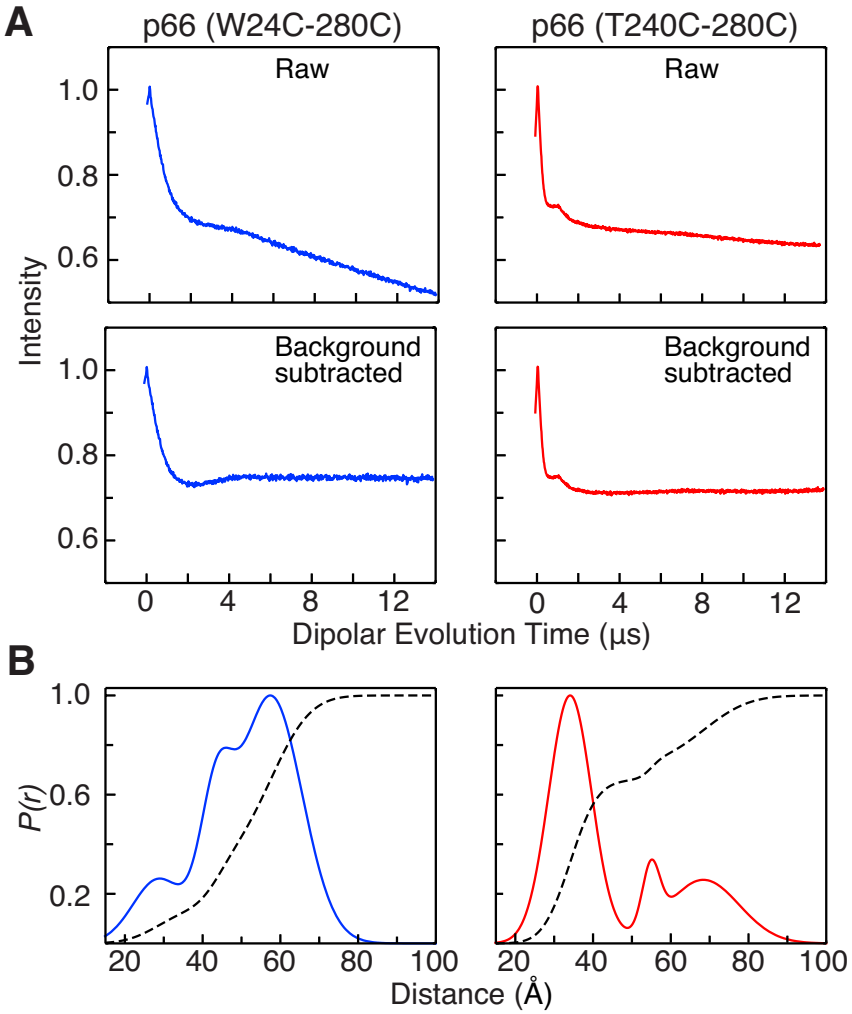

Figure S8. DEER echo curves and $P(r)$ distance distributions for HIV-1 reverse transcriptase using ghost peak suppression via power scaling. **(A)** Raw (top) and background subtracted (bottom) DEER echo curves for p66 (W24C/C280) and p66 (W240C/C280) in 50% (v/v) d8-glycerol obtained with ELDOR pulse flip angle of ~75 and ~65°, respectively, corresponding to normalized modulation depth Δ/Δ_{max} values of 0.51 and 0.45, respectively (The ELDOR pulse length employed was 8 ns in both cases with attenuation settings of 21 and 22 dB, respectively). Previous work on organic tetra-radicals has shown that the use of an ELDOR pulse flip angle corresponding to $\Delta/\Delta_{max} \sim 0.5$ effectively suppresses ghost peaks in systems comprising more than two spins.[S11] (Note that multispin effects do not impact the normalized modulation depth.) Other experimental settings were the same as those reported for the DEER curves shown in Fig. S4, except that the dipolar evolution curve was sampled up to t_{max} = 15 μs with τ_2 set to (t_{max} + 700 ns), and Δt = 20 ns. Data acquisition time was ~ 16h. The DD homogeneous model with a dimension of 3 (i.e. exponential background)[S10] was used to fit and subtract the background. (**B**) $P(r)$ distance distributions derived from the DEER data using the program GLADD with three Gaussians.[S10] A cutoff of 14 μs was used to process both data sets. The optimal number of Gaussians was judged by χ^2, Akaike, and distribution of residuals criteria.[S10] The dashed lines represent the integrated intensities of the three Gaussians. The $P(r)$ distance distributions contain contributions from both monomer and dimer.

Table S1 Comparison of monomer-dimer populations of 50 μM (in subunits) p66 determined by sedimentation velocity and inversion modulated DEER EPR.

Glycerol (v/v %)	DEER EPR		Sedimentation velocity[a]					
			Monomer			Dimer		
	monomer pop. (%)	dimer pop (%)	signal ($\%A_{250}$)	concn. (μM)	pop. (%)	signal ($\%A_{250}$)	concn. (μM)	pop. (%)
10			20.3±0.4	10±0.2	33	79.7±0.4	20±0.1	67
30[b]	54	46	26.5±0.4	13±0.5	42	73.5±0.4	18±0.5	58
50[b]	65	36	55±2	28±1	71	45±2	11±0.5	29

[a]The results of sedimentation velocity are based on absorbance $c(s)$ profiles. These only consider contributions from the major monomer and dimer species. Dimer concentrations are presented in terms of dimer units. The errors represent the standard deviations resulting from the fits, and thus provide a measure of precision and not accuracy which is comprised to some extent not only by the simplifications in the analysis but also by the complexity introduced from the dynamic gradient arising from the co-sedimentation of glycerol.

[b]Optimal sedimentation velocity data fits are observed at slightly lower glycerol concentrations than stated reflecting possible pipetting errors. This, along with the fact that fully deuterated d_8-glycerol (used in the EPR experiments) is denser than regular protonated glycerol used in the sedimentation velocity experiments, may explain the differences in the monomer-dimer populations reported by DEER EPR and sedimentation velocity, as the latter (but not the former) will be influenced by the density of the medium.

Supplementary references

[S1] M. Lapkouski, L. Tian, J. T. Miller, S. F. Le Grice, W. Yang, *Nature Struct. Mol. Biol.* **2013**, *20*, 230-236.

[S2] O. Kensch, T. Restle, B. M. Wohrl, R. S. Goody, H. J. Steinhoff, *J. Mol. Biol.* **2000**, *301*, 1029-1039.

[S3] J. L. Baber, J. M. Louis, G. M. Clore, *Angew Chem Int Ed Engl* **2015**, *54*, 5336-5339.

[S4] H. Zhao, C. A. Brautigam, R. Ghirlando, P. Schuck, *Curr. Protocols Prot. Sci.* **2013**, *20*, unit 20.12.

[S5] R. Ghirlando, A. Balbo, G. Piszczek, P. H. Brown, M. S. Lewis, C. A. Brautigam, P. Schuck, H. Zhao, *Anal. Biochem.* **2013**, *440*, 81 – 95.

[S6] P. Schuck, *Biophys. J.* **2000**, *78*, 1601 – 1619.

[S7] P. Schuck, *Biophys. Chem.* **2004**, *108*, 187 – 200.

[S8] J. L. Cole, J. W. Lary, T. P. Moody, T. Laue, *Methods Cell Biol.* **2008**, *84*, 143 – 179.

[S9] G. Jeschke, M. Sajid, M. Schulte, A. Godt, *Phys. Chem. Chem. Phys.* **2009**, *11*, 6580-6591.

[S10] S. Brandon, A. H. Beth, E. J. Hustedt, *J. Magn. Reson.* **2012**, *218*, 93-104.

[S11] T. von Hagens, Y. Polyhach, M. Sajid, A. Godt, G. Jeschke, *Phys. Chem. Chem. Phys.* **2013**, *15*, 5854-5866.

[S12] C. Ebel, H. Eisenberg, R. Ghirlando, *Biophys. J.* **2000**, *78*, 385 – 393.

[S13] A. Priev, A. Almagor, S. Yedgar, B. Gavish, *Biochemistry* **1996**, *35*, 2061 – 2066.